GaN-Based Ultraviolet Phototransistor With Two Parallel Polarization-Doped Junctions and an $Al_{0.20}Ga_{0.80}N$ Insertion Layer to Achieve Low Dark Current and High Detectivity

Zhan Xuan, Chunshuang Chu, Kangkai Tian, Zhengji Zhu, Zhiwei Xie, Ke Jiang, Yonghui Zhang, Xiaojuan Sun, Zi-Hui Zhang, and Dabing Li

***Abstract*— In this report, a polarization-doped n-p-i-p-n GaN/$Al_xGa_{1-x}N$/GaN ultraviolet phototransistor with an $Al_{0.20}Ga_{0.80}N$ insertion layer is proposed. The $Al_xGa_{1-x}N$ layer with graded AlN composition is utilized as a p-type layer. The $Al_{0.20}Ga_{0.80}N$ insertion layer is embedded into the unintentionally doped GaN (i-GaN) absorption layer, which can increase the conduction band barrier height and reduce the electron leakage from the substrate for the device. As a result, the dark current lower than 3.40×10^{-11} A/cm^2 can be obtained. When the device is illuminated with ultraviolet light, the forward biased junction facilitates the photo-generated carrier transport. As a result, a photo-to-dark-current ratio (PDCR) larger than 10^4 at the applied bias of 5 V is realized. The carriers are transported in the region far apart from the device surface, and this gives rise a response with the rise time of 27 ms and decay time of 44 ms, respectively.**

***Index Terms*— Carrier transport, dark current, graded AlN composition, insertion layer, ultraviolet phototransistor.**

Manuscript received 8 August 2023; accepted 24 August 2023. Date of publication 13 September 2023; date of current version 24 October 2023. This work was supported in part by the National Key Research and Development Program of China under Grant 2022YFB3605102; in part by the National Natural Science Foundation of China under Grant 62074050, Grant 61975051, and Grant 62275073; in part by the China Postdoctoral Science Foundation under Grant 2022M720983; in part by the Science and Technology Program of Hebei under Grant 215676146H and Grant 225676163GH; and in part by the State Key Laboratory of Reliability and Intelligence of Electrical Equipment, Hebei University of Technology under Grant EERIPD2021012. The review of this article was arranged by Editor J. Zhang. *(Zhan Xuan and Chunshuang Chu contributed equally to this work.) (Corresponding authors: Zi-Hui Zhang; Kangkai Tian.)*

Zhan Xuan, Chunshuang Chu, Zhengji Zhu, Yonghui Zhang, and Zi-Hui Zhang are with State Key Laboratory of Reliability and Intelligence of Electrical Equipment, Tianjin 300401, China, and also with School of Electronics and Information Engineering, Hebei University of Technology, Key Laboratory of Electronic Materials and Devices of Tianjin, Tianjin 300401, China (e-mail: zh.zhang@hebut.edu.cn).

Kangkai Tian is with the School of Integrated Circuits, Guangdong University of Technology, Guangzhou 510006, China (e-mail: kk_tian@gdut.edu.cn).

Zhiwei Xie, Ke Jiang, Xiaojuan Sun, and Dabing Li are with State Key Laboratory of Luminescence and Applications, Changchun Institute of Optics, Fine Mechanics and Physics, Chinese Academy of Sciences, Changchun 130033, China.

Color versions of one or more figures in this article are available at https://doi.org/10.1109/TED.2023.3310944.

Digital Object Identifier 10.1109/TED.2023.3310944

I. Introduction

Ultraviolet photodetectors (UV PDs) have been widely used in military and civilian applications, such as missile warning, non-line-of-sight communications, flame detection, and environmental monitoring [1], [2], [3], [4]. Most of these applications require devices with high signal-to-noise ratio and high sensitivity for effective implementation. Therefore, photodetectors require high responsivity, fast response speed, and low dark current. Till now, attempts have been made to improve the responsivity and sensitivity for photodetectors made of III–V nitrides, such as a AlGaN/GaN-based phototransistor with a peak responsivity of 1.52×10^5 A/W at the wavelength of 265 nm [5], an ultrasensitive AlGaN-based UV PD having a peak detectivity of 1.5×10^{18} Jones at the wavelength of 260 nm [6], and a 92% external quantum efficiency (EQE) for 289-nm p-i-n AlGaN PD with AlN-graded p-AlGaN ohmic contact layer [7]. Moreover, GaN-based UV PDs detecting optical signal at the wavelength ranging from 300 to 400 nm has also been reported, such as a polarization-enhanced p-i-n AlGaN PD achieving a peak responsivity of 0.086 A/W at the wavelength of 302 nm [8] and a UV PD based on p-GaN/AlGaN/GaN heterostructures possessing a photo-to-dark current ratio (PDCR) over 10^8 at the wavelength of 365 nm [9]. Therefore, (Al)GaN-based UV PDs have the advantages of working in different band ranges by adjusting the Al composition [10]. Among the candidates for UV PDs, p-i-n-structured UV PDs overwhelm other structures (e.g., MSM PDs) in high quantum efficiency, low dark current, and fast response speed [11]. This is attributed to the fact that p-i-n UV PDs have strong built-in electric field in the absorption layer [12]. Moreover, unlike MSM UV PDs, the photon-generated carriers for p-i-n UV PDs are more likely to transport in the bulk region rather than in the surface region [13]. Hence, the carriers are less affected by any surface traps, which also enables p-i-n UV PDs to have faster response speed [14].

(Al)GaN-based p-i-n UV PDs still have challenges in both material growth and p-type doping engineering. On the one hand, the adoption of Mg dopants in the epitaxial layer will inevitably cause defects that behave as "killers" for both photons and carriers [15], [16]. Moreover, epitaxial layer grown on the p-type (Al)GaN layer will possess rough surface and poor crystalline quality [17]. Hence, most reports regarding (Al)GaN-based p-i-n UV PDs have the p-GaN layer grown lastly [18]. On the other hand, p-type (Al)GaN layer has a low Mg-doping efficiency [19]. The low p-type doping efficiency in the p-type (Al)GaN layer cannot generate very strong build-in electric field in the unintentionally GaN absorption layer (i-GaN). This will result in the poor carrier generation rate and the current transport. Fortunately, the electric field magnitude in the absorption layer can be enhanced if the polarization effect is applied, which effectiveness has been demonstrated in (Al)GaN-based p-i-n UV PDs [20]. The polarization-induced p-type base region has also been designed and reported [21], such that a n-p-n phototransistor is demonstrated. The electric field in the optical absorption layer is also influenced by the intrinsic absorption layer for p-i-n UV PDs [22]. A thick intrinsic layer is required, so that more light can be absorbed. Nevertheless, the increased thickness for the absorption layer may decrease the electric field magnitude. This will sacrifice the generation rate for electrons and holes [23]. However, we believe that when multiple parallel junctions are designed and fabricated, the area for the absorption layer can be further increased and the strong electric field magnitude in the absorption layer can also be maintained.

Hence, in this work, we take the advantage of the polarization effect by grading the AlN composition for the AlGaN layer, so that a polarization-induced p-type AlGaN can be formed [24]. We also design and fabricate two parallel junctions, i.e., n-p-i-p-n phototransistors, so that the absorption area can be doubled, which helps to increase the photocurrent. To suppress the carrier leakage from the substrate for the proposed n-p-i-p-n phototransistors with two parallel junctions, we also grow an $Al_{0.20}Ga_{0.80}N$ insertion layer below the unintentionally n-typed doped (i-GaN) layer serving as the energy barrier layer. Very importantly, the negative polarization-induced interface charges are generated at the i-GaN/$Al_{0.20}Ga_{0.80}N$ interface, and this further prevents the electron injection downward into the substrate layer. As a result, the leakage level for the photo-generated carriers can be significantly reduced. If the device is operated in dark condition, such $Al_{0.20}Ga_{0.80}N$ insertion layer helps to suppress the defect-related leakage current from the substrate. This will significantly decrease the dark current level.

II. Structure Design and Simulation Models

A. Device Design and Simulation

The 3-D schematic of the proposed device structure is shown in Fig. 1(a). The carrier transport process is also illustrated, such that the cathode collects holes and the anode collects electrons when the device is illuminated by UV light. Fig. 1(b) is the energy band diagram for an n-p-i-p-n structure under equilibrium. The p-type region is the AlGaN layer with graded Al composition that has negative polarization

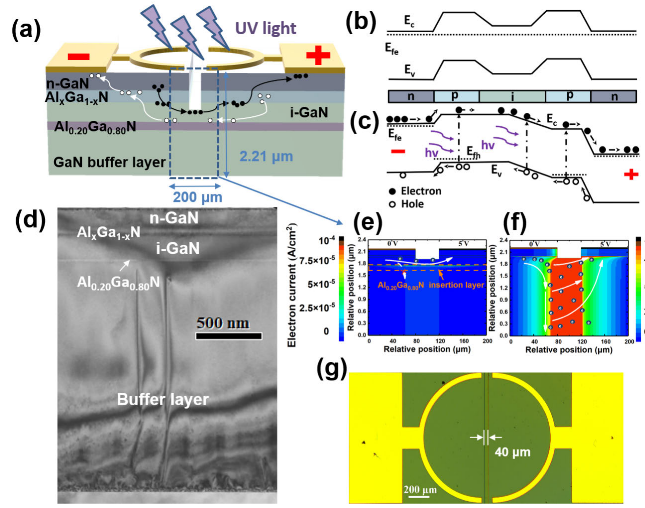

Fig. 1. (a) Schematic for the n-p-i-p-n GaN/$Al_xGa_{1-x}N$/GaN UV phototransistor. Schematic energy band diagrams for the proposed device (b) at equilibrium and (c) in biased condition. (d) Cross-sectional TEM image for n-p-i-p-n regions. Two-dimensional profiles of the electron current for (e) UV phototransistor with $Al_{0.20}Ga_{0.80}N$ insertion layer and (f) without $Al_{0.20}Ga_{0.80}N$ insertion layer at the bias of 5 V in dark condition, respectively. (g) Top view of the fabricated n-p-i-p-n GaN/$Al_xGa_{1-x}N$/GaN UV phototransistor.

induced bulk charges. When the device is biased, as shown in Fig. 1(c), the left p-n and right p-i junctions are forwardly biased, while the right p-n and left p-i junctions are reversely biased. If the device is in the dark condition, then those reversely biased junctions will not allow the flow for any minority carriers. Therefore, our proposed phototransistor is in the OFF-state and may have a very low dark current. Once upon being illuminated by UV light, the nonequilibrium carriers will be generated in the i-GaN region. Moreover, the i-GaN region between the two mesas [see Fig. 1(a)] has also photo-generated carriers, which serves as the "gate" and then turns on the transistor. The photogenerated electrons and holes will be transported to the anode and cathode, respectively. As a result, a high-level photocurrent will be generated. As shown in Fig. 1(d), we present the cross-sectional TEM image for the proposed structure. It can be seen that the thicknesses of the epitaxial layers are precisely controlled and excellent crystalline quality can be obtained in the $Al_{0.20}Ga_{0.80}N$ insertion layer, the i-GaN layer, the $Al_xGa_{1-x}N$ layer, and the top n-GaN layer.

To better understand the device physics for carrier generation and carrier transport, numerical simulations are conducted by using SinoTCAD software, which can calculate energy band, current–voltage (I–V) characteristics, electric field, and current distribution by solving the continuity and Poisson's equations. The absorption coefficients of AlGaN and GaN materials at different wavelengths can be found in [25]. The polarization effect is considered at the $Al_xGa_{1-x}N$/GaN and $Al_{0.20}Ga_{0.90}N$/GaN heterojunctions, for which the polarization sheet charge density is set to $\sim 5.93 \times 10^{16}$ m^{-2} and $\sim 4.21 \times 10^{16}$ m^{-2}, respectively, and a negative polarization bulk charge density of $\sim 9.48 \times 10^{17}$ cm^{-3} has been assumed in the $Al_xGa_{1-x}N$ region [26], [27], [28]. It is worth mentioning that our fabricated device is too large to be calculated by our simulator. Considering the in-plane symmetric feature for the fabricated device, we set the simulated region with the width of 200 μm in our physical model. We first calculate and present 2-D profile of the electron current for the device in Fig. 1(a) at the bias of 5 V in the dark condition [see Fig. 1(e)]. For comparison, the 2-D profiles of the electron current are also calculated for the device if no $Al_{0.20}Ga_{0.80}N$ insertion layer is adopted in Fig. 1(f). The comparison shows that the $Al_{0.20}Ga_{0.80}N$ insertion layer can effectively suppress the leakage electron current that is generated by the dislocation/defects in the GaN buffer layer [see Fig. 1(d)]. Hence, we can speculate that the $Al_{0.20}Ga_{0.80}N$ insertion layer significantly reduces the dark current for the proposed phototransistor. Fig. 1(g) demonstrates the microscopic graph for the top view of the fabricated n-p-i-p-n phototransistor.

B. Device Fabrication

The proposed phototransistor is grown by using metal–organic chemical vapor deposition (MOCVD) on a 500-μm-thick sapphire substrate. First, a GaN nucleation layer with a thickness of 20 μm is grown on the sapphire substrate. Next, a 1.8-μm-thick GaN buffer layer is grown on the nucleation layer. After that, an $Al_{0.20}Ga_{0.80}N$ insertion layer with a thickness of 10 nm is grown, on which an absorption layer of 200-nm i-GaN is further deposited serving as the absorption layer. A 50-nm-thick $Al_xGa_{1-x}N$ layer is subsequently deposited, for which the AlN composition is linearly varied from 0.27 to 0 along the [0001] growth orientation. Finally, a 150-nm-thick n-GaN layer with an n-type doping concentration of 3.5×10^{18} cm^{-3} is grown. After completing the epitaxial growth, the n-GaN and $Al_xGa_{1-x}N$ layers are dry etched by using an inductively coupled plasma (ICP) etching system with a depth of 250 nm to form grooves with a width of 40 μm. Two Ti/Al/Ti/Au (20/30/60/100 nm) ohmic contacts are deposited on the n-GaN layer on both mesa by utilizing e-beam system.

C. Characterization and Measurement

The structural properties are characterized by utilizing high-resolution field-emission transmission electron microscope (JEM-2100F). The I–V characteristics are measured by using Keithley 6487. The spectral responses are measured by using a DSR100 system with a xenon lamp, chopper, monochromator, Keithley 6487, SR830 lock-in amplifier, and standard Si detector. The transient response spectra are measured by using a RIGOL DS6104 digital oscilloscope. A pulsed laser with an emission wavelength of 310 nm is used to measure the photocurrent and transient responses.

III. Results and Discussion

Fig. 2(a) presents the measured current in terms of the applied bias both in dark and illumination conditions for the proposed n-p-i-p-n phototransistor. The dark current value is beyond the scope of our measurement system. Hence, the precise value for the dark current is not able to be characterizable at the current stage. However, we estimate that the dark current is lower than 3.40×10^{-11} A/cm^2 at

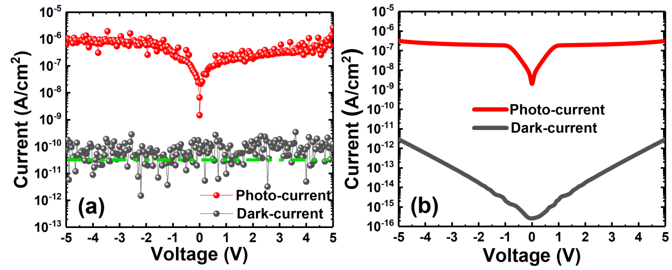

Fig. 2. Dark current and photocurrent in terms of the applied bias from (a) experimental measurement and (b) numerical calculation.

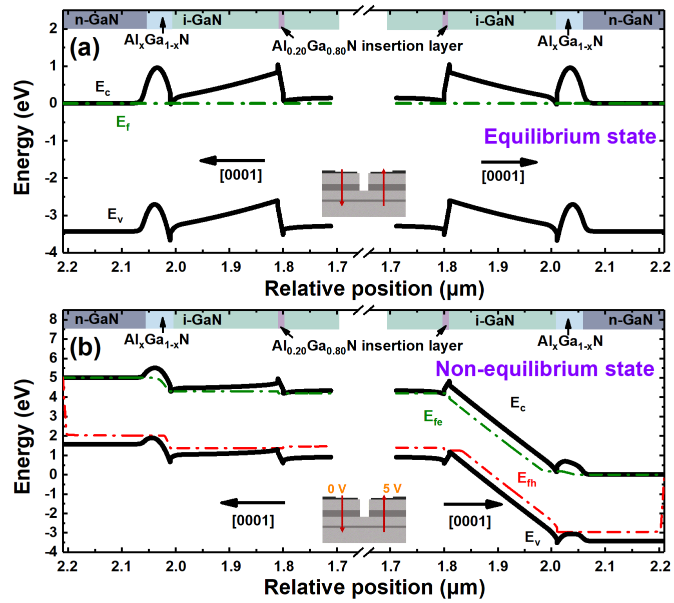

Fig. 3. Energy band alignment for the proposed device at (a) equilibrium and (b) bias of 5 V in the 310-nm illumination condition.

the applied bias from -5 to 5 V. When the UV light of 310-nm wavelength and 48-μW/cm^2 intensity is applied to the device, the photocurrent can reach 10^{-6} A/cm^2 at the applied bias of 5 V. The proposed device shows a PDCR larger than 10^4. We also calculate the dark current and photocurrent at different applied biases, which are shown in Fig. 2(b). The comparison between Fig. 2(a) and (b) illustrates that our measured and calculated photocurrent are of the same level, which validates the effectiveness for our physical models. Fig. 2(b) also presents that the theoretical dark current can be as low as 10^{-15} A/cm^2. The theoretical PDCR is estimated to be as large as 10^7. We believe that the high PDCR value originates from forwardly biased p-n junctions in the proposed phototransistor, which favors the transport for the minority carriers. In the meanwhile, the extremely low dark current value is attributed to the $Al_{0.20}Ga_{0.80}N$ insertion layer that suppresses the leakage electron current from the substrate [see Fig. 1(e)].

To further reveal the carrier transport mechanism, we calculate the energy band alignment for the proposed device. Fig. 3(a) shows the symmetric energy band diagrams for the two mesas at equilibrium. Here, the $Al_xGa_{1-x}N$ with graded AlN composition has negative polarization-induced bulk charges, and hence, it serves as a p-type layer. The energy

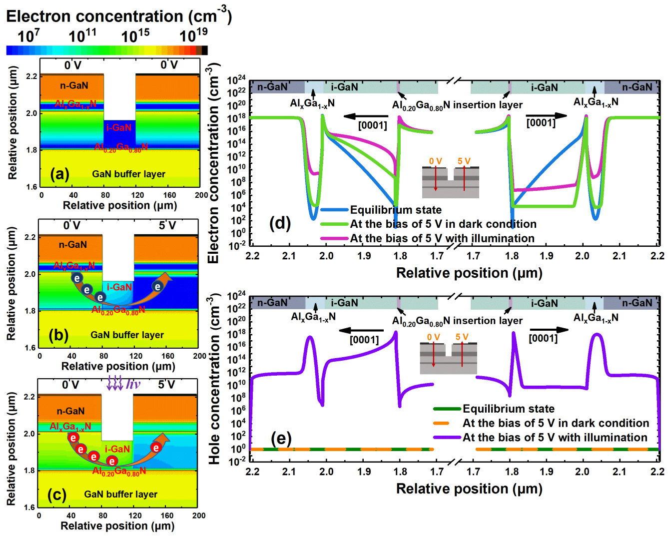

Fig. 4. Two-dimensional profiles of the electron concentration for the proposed device (a) at equilibrium, (b) in dark condition, and (c) under 310-nm illumination at the bias of 5 V. One-dimensional profiles of (d) electron and (e) hole concentration near the top of the proposed device at the equilibrium and nonequilibrium state, respectively.

barrier layer by $Al_{0.20}Ga_{0.80}N$ layers to suppress the leakage electron current from the substrate region is also observed. Fig. 3(b) shows the calculated energy band diagram for the two mesas when the bias of 5 V in applied in the right mesa. Being consistent with the experimental condition, the wavelength of the incident light is set to 310 nm. The p-n junction in the left mesa is forwardly biased, which promises high-efficiency current flow across the i-GaN layer for the photo-generated minority carriers. If we refer to the right mesa region, it seems that the i-GaN layer in the right mesa is more bent when compared to that in the left mesa. This originates from the build-in electric field in the reversely biased p-n junction for the right mesa. The function of the i-GaN layer in the right mesa includes carrier generation by the 310-nm incident light and the high-level current flow across the reversely biased p-n junction. As a result, Fig. 3(a) and (b) agrees with Fig. 2(a) and (b), such that the proposed phototransistor in this work has the advantage of possessing extremely low dark current and the large photocurrent.

Fig. 4(a) shows the 2-D electron concentration profiles in dark condition when the device is unbiased. The electron concentration in the i-GaN layer has the electron concentration lower than 10^{14} cm^{-3}. More importantly, if we look into the i-GaN region between the two mesas, the electron concentration therein is even lower than 10^{5} cm^{-3}. This is caused by the repulsive effect of negatively polarized interface charges at the i-GaN/$Al_{0.20}Ga_{0.80}N$ interface. Fig. 4(b) demonstrates the 2-D electron concentration at the bias of 5 V in the dark condition. The electron concentration in the i-GaN region between the two mesas become lower than 10^{8} cm^{-3}. Hence, such low electron concentration therein still helps turn off the device in dark condition. Fig. 4(c) shows the 2-D electron concentration profiles at the bias of 5 V when the 310-nm incidence light is turned on. Then, the electron concentration in the i-GaN region between the two mesas is higher than 10^{15} cm^{-3}, which turns on the device. Meanwhile, it agrees with Fig. 3(b) that the i-GaN layer region generates nonequilibrium electrons. The even stronger electric field in the i-GaN region for the right mesa also significantly facilitates the electron transport and electron collection at the anode region. For even better illustrating the carrier distribution, we show the 1-D distribution for both electrons and holes in Fig. 4(d) and (e), respectively. It is noted that the hole concentration is very low in dark condition because of the unintentionally n-type doping effect in the i-GaN layer. However, upon the 310-nm illumination, we can see that the nonequilibrium hole concentration is of the same level for the nonequilibrium electron concentration. This means that the 310-nm incident light generates electron–hole pairs, and the proposed phototransistor here is a bipolar device. The 1-D electron concentration profiles are consistent with that in Fig. 4(a)–(c). Fig. 4(d) and (e) further shows the importance of the i-GaN layer in the right mesa, such that the i-GaN layer therein significantly favors the transport for both electrons and holes due to the even stronger electric field in the i-GaN layer. It is vice versa if the left mesa is biased to 5 V. Then, the stronger electric field in the i-GaN layer for the left mesa can be obtained. Correspondingly, the proposed UV phototransistor can be sensitive to UV light in both quadrants.

Fig. 5(a) and (b) shows the measured spectral responsivity and the detectivity under the light wavelength of 250–400 nm and different biases. The bias is increased from 1 to 3 V, and the responsivity gets enhanced with the increased bias. The proposed phototransistor can detect the light in the UV and deep UV spectral regions. At the bias of 3 V, the peak responsivity can reach 40.6 mA/W. The UV/visible ($R_{314\,\mathrm{nm}}/R_{400\,\mathrm{nm}}$) rejection ratio values are 34, 334, and 124 at the biases of 1, 2, and 3 V, respectively. We also present the detectivity, which is derived by using the following equation [29]:

$$D^* = R \Big/ \sqrt{\frac{2eI_d}{S}} \qquad (1)$$

where R is the responsivity, S is the effective area of photodetector, e is the free electron charge, and I_d is the dark current. Here, R can be obtained by Fig. 5(a), and S is 0.0156 cm^2 for our device. As we have mentioned before, the dark current of the proposed phototransistor is too low to be testable by our equipment. Hence, we estimated I_d/S to be 3.23×10^{-11} A/cm^2 by assuming the dark current of 5.04×10^{-13} A according to Fig. 2(a). Then, the detectivity at different biases is shown in Fig. 5(b), and the peak detectivity of 1.26×10^{13} Jones at a low bias of 3 V. We believe that we have underestimated the values for the detectivity. Fig. 5(c) shows the time-dependent response current at the 2 V bias. We use the fast Fourier transform (FFT) filter to fit the tested data. By following the calculation criteria in [30], we obtain a rise time (τ_r) of 27 ms and a decay time (τ_d) of 44 ms for the fabricated phototransistor in this work. Because of the low mobility of holes, we believe that the response speed for our phototransistor can be further increased if the photo-generated holes can be consumed [31]. We also compare the device performances, including detectivity, response speed, PDCR, and dark current of our device along with other reported (Al)GaN-based p-i-n UV PDs in Table I. It shows that our fabricated device shows comparable results when compared

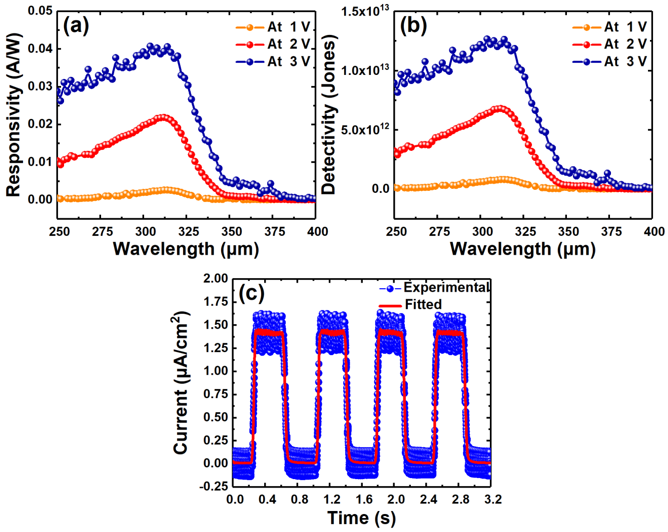

Fig. 5. (a) Measured spectral responsivity and (b) detectivity in terms of different incident light wavelengths at the applied biases of 1, 2, and 3 V, respectively. (c) Time-dependent optical response for the designed device at 2-V bias when a 310-nm UV illumination signal is applied.

TABLE I
DETECTOR PERFORMANCE FOR THE REPORTED (Al)GaN-BASED p-i-n UV PDs IN THE LITERATURE

Material structure	Wavelength (nm)	D* (Jones)	τ_r/τ_d (ms)	PDCR	I_d (A/cm^2)	Ref
$Al_{0.40}Ga_{0.60}N$ p-i-n	289	3.33×10^{13} (0 V)	<13 (0 V)	>10^6 (-10 V)	1.00×10^{-9} (-10 V)	[7]
GaN p-i-n	348	1.14×10^{12} (0 V)	-/-	>10^3 (0 V)	<1.00×10^{-7} (0V)	[13]
GaN p-i-n-i-p	358	6.44×10^{14} (5 V)	1.07/ 1.16 (5 V)	~10^5 (5 V)	<1.03×10^{-9} (5 V)	[18]
$Al_{0.30}Ga_{0.70}N$ p-i-n	304	3.85×10^{12} (-20 V)	-/-	270 (-20 V)	1.70×10^{-9} (-1 V)	[20]
$Al_{0.40}Ga_{0.60}N$ p-i-n	275	>6.95×10^{12} (-5 V)	-/-	-	<2.00×10^{-9} (-10 V)	[32]
$Al_{0.40}Ga_{0.60}N$ p-i-n	260	>3.50×10^{11} (-5 V)	-/-	-	<6.90×10^{-8} (-5 V)	[33]
$Al_{0.40}Ga_{0.60}N$ p-i-n	289	>1.57×10^{13} (0 V)	<13 (0 V)	4.8×10^5 (0 V)	3.60×10^{-9} (-2 V)	[34]
GaN p-i-n	360	2.19×10^{13} (0 V)	0.075/ 0.11 (-5 V)	8.3×10^5 (0 V)	~0.80×10^{-9} (0 V)	[35]
$Al_{0.38}Ga_{0.62}N$ p-i-n-i-n	290	1.60×10^{12} (0 V)	-/-	-	3.00×10^{-8} (0 V)	[36]
GaN/AlGaN n-p-i-p-n	314	>1.26×10^{13} (3V)	27/44 (2 V)	>10^4 (5 V)	<3.40×10^{-11} (3 V)	This work

with other reports. Nevertheless, our dark current shows the smallest value.

IV. CONCLUSION

In conclusion, a n-p-i-p-n GaN/Al_xGa_{1-x}N/GaN ultraviolet phototransistor with low dark current and high detectivity has been designed, simulated, fabricated, and investigated. The reversely biased p-n junction and the i-GaN layer in the n-p-i-p-n GaN/Al_xGa_{1-x}N/GaN ultraviolet phototransistor enable the device to possess excellent OFF-state capability. We also purposely grown an $Al_{0.20}Ga_{0.80}$N insertion layer between the buffer i-GaN layer and the absorptive i-GaN layer. By doing so, the electron leakage level from the buffer i-GaN into the absorptive i-GaN layer can be decreased. Therefore, the dark current is lower than 3.40×10^{-11} A/cm^2, and the PDCR value is larger than 10^4 at a bias of 5 V. A peak detectivity of higher than 1.26×10^{13} Jones can be obtained at the bias of 3 V in the UV range. We also point out that our demonstrated device has a high hole generation rate. If the holes can be consumed by, e.g., radiative recombination, we believe that the response speed for the device can potentially have a rise time shorter than 27 ms and decay time shorter than 44 ms. We believe that the reported device in this work inspires the UV community to fabricate more efficient UV-sensitive semiconductor materials and devices. The reported device physics here also provides more understanding for photosensitive devices.

REFERENCES

[1] R. Tang et al., "Ga_2O_3/GaN heterostructural ultraviolet photodetectors with exciton-dominated ultranarrow response," *ACS Appl. Electron. Mater.*, vol. 4, no. 1, pp. 188–196, Jan. 2022, doi: 10.1021/acsaelm.1c00917.

[2] J. Sun et al., "A high responsivity and controllable recovery ultraviolet detector based on a WO_3 gate AlGaN/GaN heterostructure with an integrated micro-heater," *J. Mater. Chem. C*, vol. 8, no. 16, pp. 5409–5416, Apr. 2020, doi: 10.1039/d0tc00553c.

[3] R. Yuan and J. Ma, "Review of ultraviolet non-line-of-sight communication," *China Commun.*, vol. 13, no. 6, pp. 63–75, Jun. 2016, doi: 10.1109/cc.2016.7513203.

[4] Y.-J. Lu, C.-N. Lin, and C.-X. Shan, "Optoelectronic diamond: Growth, properties, and photodetection applications," *Adv. Opt. Mater.*, vol. 6, no. 20, Oct. 2018, Art. no. 1800359, doi: 10.1002/adom.201800359.

[5] L. Yang et al., "Temperature-dependent photodetection behavior of AlGaN/GaN-based ultraviolet phototransistors," *Appl. Phys. Lett.*, vol. 120, no. 9, Feb. 2022, Art. no. 091103, doi: 10.1063/5.0083171.

[6] J. Lu, Z. Lv, X. Qiu, S. Lai, and H. Jiang, "Ultrasensitive and high-speed AlGaN/AlN solar-blind ultraviolet photodetector: A full-channelself-depleted phototransistor by a virtual photogate," *Photon. Res.*, vol. 10, no. 9, pp. 2229–2238, Sep. 2022, doi: 10.1364/prj.467689.

[7] A. Kalra, S. Rathkanthiwar, R. Muralidharan, S. Raghavan, and D. N. Nath, "Polarization-graded AlGaN solar-blind p-i-n detector with 92% zero-bias external quantum efficiency," *IEEE Photon. Technol. Lett.*, vol. 31, no. 15, pp. 1237–1240, Aug. 1, 2019, doi: 10.1109/lpt.2019.2923147.

[8] L.-H. Yang, K.-R. Lai, B.-H. Zhang, X.-L. Fu, J.-J. Wang, and W. Wei, "Polarization enhanced photoresponse of AlGaN p-i-n photodetectors," *Phys. Status Solidi A*, vol. 212, no. 3, pp. 698–702, Mar. 2015, doi: 10.1002/pssa.201431506.

[9] Q. Lyu, H. Jiang, and K. M. Lau, "High gain and high ultraviolet/visible rejection ratio photodetectors using p-GaN/AlGaN/GaN heterostructures grown on Si," *Appl. Phys. Lett.*, vol. 117, no. 7, Aug. 2020, Art. no. 071101, doi: 10.1063/5.0011685.

[10] D. Li, K. Jiang, X. Sun, and C. Guo, "AlGaN photonics: Recent advances in materials and ultraviolet devices," *Adv. Opt. Photon.*, vol. 10, no. 1, pp. 43–110, Mar. 2018, doi: 10.1364/AOP.10.000043.

[11] Z. Alaie, S. M. Nejad, and M. H. Yousefi, "Recent advances in ultraviolet photodetectors," *Mater. Sci. Semicond. Process.*, vol. 29, pp. 16–55, Jan. 2015, doi: 10.1016/j.mssp.2014.02.054.

[12] C. Xie et al., "Recent progress in solar-blind deep-ultraviolet photodetectors based on inorganic ultrawide bandgap semiconductors," *Adv. Funct. Mater.*, vol. 29, no. 9, Feb. 2019, Art. no. 1806006, doi: 10.1002/adfm.201806006.

[13] P. Dalapati, K. Yamamoto, T. Kubo, T. Egawa, and M. Miyoshi, "Bias-controlled photocurrent generation process in GaN-based ultraviolet p–i–n photodetectors fabricated with a thick Al_2O_3 passivation layer," *Optik*, vol. 245, Nov. 2021, Art. no. 167691, doi: 10.1016/j.ijleo.2021.167691.

[14] L. Shi et al., "Status and outlook of metal–inorganic semiconductor–metal photodetectors," *Laser Photon. Rev.*, vol. 15, no. 1, Jan. 2021, Art. no. 2000401, doi: 10.1002/lpor.202000401.

[15] N. Tetsuo, I. Nobuyuki, T. Kazuyoshi, K. Keita, and K. Tetsu, "Wide range doping control and defect characterization of GaN layers with various Mg concentrations," *J. Appl. Phys.*, vol. 124, no. 16, Oct. 2018, Art. no. 165706, doi: 10.1063/1.5045257.

[16] R. Kirste, B. Sarkar, P. Reddy, Q. Guo, R. Collazo, and Z. Sitar, "Status of the growth and fabrication of AlGaN-based UV laser diodes for near and mid-UV wavelength," *J. Mater. Res.*, vol. 36, no. 23, pp. 4638–4664, Dec. 2021, doi: 10.1557/s43578-021-00443-8.

[17] J. Ran et al., "Study on Mg memory effect in npn type AlGaN/GaN HBT structures grown by MOCVD," *Microelectron. J.*, vol. 37, no. 7, pp. 583–585, Jul. 2006, doi: 10.1016/j.mejo.2005.10.001.

[18] K. Jiang et al., "Three-dimensional metal–semiconductor–metal bipolar ultraviolet phototransistor based on GaN p-i-n epilayer," *Appl. Phys. Lett.*, vol. 119, no. 16, Oct. 2021, Art. no. 161105, doi: 10.1063/5.0064779.

[19] K. Jiang et al., "Quantum engineering of non-equilibrium efficient p-doping in ultra-wide band-gap nitrides," *Light, Sci. Appl.*, vol. 10, no. 1, p. 69, Mar. 2021, doi: 10.1038/s41377-021-00503-y.

[20] Q. Hou et al., "A high quantum efficiency narrow-band UV-B AlGaN p-i-n photodiode with polarization assistance," *IEEE Photon. J.*, vol. 13, no. 3, pp. 1–8, Jun. 2021, doi: 10.1109/JPHOT.2021.3086855.

[21] L. Sun, Z. Lv, Z. Zhang, X. Qiu, and H. Jiang, "High-performance AlGaN heterojunction phototransistor with dopant-free polarization-doped p-base," *IEEE Electron Device Lett.*, vol. 41, no. 3, pp. 325–328, Mar. 2020, doi: 10.1109/LED.2020.2966917.

[22] Z. Cao, D. Zhao, F. Liang, and Z. Liu, "Fabrication of high quantum efficiency p-i-n AlGaN detector and optimization of p-layer and I-layer thickness," *Mater. Res. Exp.*, vol. 7, no. 11, Nov. 2020, Art. no. 115902, doi: 10.1088/2053-1591/abca6e.

[23] X. D. Wang, W. D. Hu, X. S. Chen, J. T. Xu, X. Y. Li, and W. Lu, "Photoresponse study of visible blind GaN/AlGaN p-i-n ultraviolet photodetector," *Opt. Quantum Electron.*, vol. 42, nos. 11–13, pp. 755–764, Oct. 2011, doi: 10.1007/s11082-011-9473-8.

[24] Z.-H. Zhang et al., "P-doping-free InGaN/GaN light-emitting diode driven by three-dimensional hole gas," *Appl. Phys. Lett.*, vol. 103, no. 26, Dec. 2013, Art. no. 263501, doi: 10.1063/1.4858386.

[25] J. F. Muth et al., "Absorption coefficient and refractive index of GaN, AlN and AlGaN alloys," *MRS Internet J. Nitride Semicond. Res.*, vol. 4, no. S1, pp. 502–507, 1999, doi: 10.1557/s1092578300002957.

[26] I. P. Smorchkova et al., "Polarization-induced charge and electron mobility in AlGaN/GaN heterostructures grown by plasma-assisted molecular-beam epitaxy," *J. Appl. Phys.*, vol. 86, no. 8, pp. 4520–4526, Oct. 1999, doi: 10.1063/1.371396.

[27] W. L. Liu, Y. L. Chen, A. A. Balandin, and K. L. Wang, "Investigation of the trap states and their effect on the low-frequency noise in GaN/AlGaN HFETs," *Proc. SPIE*, vol. 5844, pp. 268–275, May 2005, doi: 10.1117/12.609571.

[28] L. Zhang et al., "Three-dimensional hole gas induced by polarization in (0001)-oriented metal-face III-nitride structure," *Appl. Phys. Lett.*, vol. 97, no. 6, Aug. 2010, Art. no. 062103, doi: 10.1063/1.3478556.

[29] X. Liu, L. Gu, Q. Zhang, J. Wu, Y. Long, and Z. Fan, "All-printable band-edge modulated ZnO nanowire photodetectors with ultra-high detectivity," *Nature Commun.*, vol. 5, no. 1, p. 4007, Jun. 2014, doi: 10.1038/ncomms5007.

[30] F. Liang et al., "Effect of Si doping on the performance of GaN Schottky barrier ultraviolet photodetector grown on Si substrate," *Photonics*, vol. 8, no. 2, p. 28, Jan. 2021, doi: 10.3390/photonics8020028.

[31] E. P. Mukhokosi and M. Maaza, "Influence of device architectures and mobility on response/recovery time of metal halide perovskites: A review," *J. Mater. Sci.*, vol. 57, no. 3, pp. 1555–1580, Jan. 2022, doi: 10.1007/s10853-021-06678-4.

[32] E. Cicek, R. McClintock, C. Y. Cho, B. Rahnema, and M. Razeghi, "$Al_xGa_{1-x}N$-based back-illuminated solar-blind photodetectors with external quantum efficiency of 89%," *Appl. Phys. Lett.*, vol. 103, no. 19, Nov. 2013, Art. no. 191108, doi: 10.1063/1.4829065.

[33] X. Li et al., "Performance comparison of front- and back-illuminated modes of the AlGaN-based p-i-n solar-blind ultraviolet photodetectors," *J. Vac. Sci. Technol. B, Nanotechnol. Microelectron., Mater., Process., Meas., Phenomena*, vol. 32, no. 3, May 2014, Art. no. 031204, doi: 10.1116/1.4871460.

[34] A. Kalra, S. Rathkanthiwar, R. Muralidharan, S. Raghavan, and D. N. Nath, "Material-to-device performance correlation for AlGaN-based solar-blind p–i–n photodiodes," *Semicond. Sci. Technol.*, vol. 35, no. 3, Mar. 2020, Art. no. 035001, doi: 10.1088/1361-6641/ab5df8.

[35] W. Xu et al., "Magnesium ion-implantation-based gallium nitride p-i-n photodiode for visible-blind ultraviolet detection," *Photon. Res.*, vol. 7, no. 8, p. B48, Aug. 2019, doi: 10.1364/prj.7.000b48.

[36] Y. Chen, Z. Zhang, Z. Li, H. Jiang, G. Miao, and H. Song, "The influence of n-AlGaN inserted layer on the performance of back-illuminated AlGaN-based p-i-n ultraviolet photodetectors," *Phys. Status Solidi A*, vol. 215, no. 2, Jan. 2018, Art. no. 1700358, doi: 10.1002/pssa.201700358.